Biophysical Journal Volume 105 September 2013 1357–1365

Spatial Configuration and Composition of Charge Modulates Transport into a Mucin Hydrogel Barrier

Leon D. Li,[†‡§] Thomas Crouzier,[‡] Aniruddh Sarkar,[§] Laura Dunphy,[‡] Jongyoon Han,[‡§] and Katharina Ribbeck[‡*]
[†]Harvard-MIT Division of Health Sciences and Technology, Cambridge, Massachusetts; [‡]Departments of Biological Engineering and [§]Electrical Engineering and Computer Science, Massachusetts Institute of Technology, Cambridge, Massachusetts

ABSTRACT The mucus barrier is selectively permeable to a wide variety of molecules, proteins, and cells, and establishes gradients of these particulates to influence the uptake of nutrients, the defense against pathogens, and the delivery of drugs. Despite its importance for health and disease, the criteria that govern transport through the mucus barrier are largely unknown. Studies with uniformly functionalized nanoparticles have provided critical information about the relevance of particle size and net charge for mucus transport. However, these particles lack the detailed spatial arrangements of charge found in natural mucus-interacting substrates, such as certain viruses, which may have important consequences for transport through the mucus barrier. Using a novel, to our knowledge, microfluidic design that enables us to measure real-time transport gradients inside a hydrogel of mucins, the gel-forming glycoprotein component of mucus, we show that two peptides with the same net charge, but different charge arrangements, exhibit fundamentally different transport behaviors. Specifically, we show that certain configurations of positive and negative charges result in enhanced uptake into a mucin barrier, a remarkable effect that is not observed with either charge alone. Moreover, we show that the ionic strength within the mucin barrier strongly influences transport specificity, and that this effect depends on the detailed spatial arrangement of charge. These findings suggest that spatial charge distribution is a critical parameter to modulate transport through mucin-based barriers, and have concrete implications for the prediction of mucosal passage, and the design of drug delivery vehicles with tunable transport properties.

INTRODUCTION

The mucus barrier is a glycoprotein gel that coats all wet surfaces in the human body, including the respiratory, gastrointestinal, and urogenital tracts. The mucus barrier has critical but poorly understood functions in protecting tissues from attacks by pathogens and toxins, while facilitating transport of beneficial particulates such as nutrients, oxygen, and sperm (1–4). The selective permeability properties of mucus have important roles in health and disease, and changes in the structure or properties of mucus can result in diseases ranging from dental cavity formation, cystic fibrosis, viral and parasitic infections, to some forms of infertility (5–9).

Little is known about the detailed molecular properties that distinguish particles that permeate, or are rejected by, a defined mucus barrier. Mucus is a complex mixture of lipids, organic components, inorganic ions, enzymes, bactericidal proteins, and the mucin glycoproteins. Mucins are the main gel-forming building blocks of mucus and are composed of threadlike core proteins, which contain large numbers of O-linked oligosaccharide chains that protrude outward. The oligosaccharide chains confer negative charge to the mucins through carboxyl and sulfate groups. The mucin protein backbone and sugars create a plethora of binding sites for many different incoming and secreted particles and cells. Our inability to predict mucus passage of designed vehicles for drug delivery, as well as natural biological substrates such as viruses, sperm cells, nutrients, or toxins is related to our poor mechanistic and quantitative understanding of how natural substrates with complex charge and hydrophobic surface properties interact with mucins.

Several studies have probed the selection criteria of the mucus barrier, using both native mucus and hydrogels from purified mucins as model systems, with uniformly functionalized nanoparticles (10–20). These studies have provided critical information about the relevance of particle size and net charge for mucus transport. However, these particles lack the rich biochemistry of natural mucus-interacting substrates, which contain charged and hydrophobic surface domains as well as specific peptide sequences in detailed spatial arrangements that may have evolved to achieve productive interactions with the mucus (21,22). Consequently, predictions of mucosal passage are difficult to achieve because current models are simplistic and fail to integrate the spatial and biochemical complexity found in natural mucus-substrate interactions. A detailed understanding of the parameters that determine fast versus slow passage through mucus will help set priorities for the design criteria of mucus-penetrating particles with targeting abilities, and, moreover, will provide new, to our knowledge, design strategies beyond the narrow focus on net charge or size of nanoparticles.

Here, we use easy-to-manipulate peptides for a systematic evaluation of microscopic surface combinations for particulate passage through a barrier of mucins. As a well-defined model for native mucus we use hydrogels generated from the natively purified mucin pig gastric MUC5AC.

Submitted May 23, 2013, and accepted for publication July 15, 2013.
*Correspondence: ribbeck@mit.edu
Editor: David Piston.

0006-3495/13/09/1357/9 $2.00
http://dx.doi.org/10.1016/j.bpj.2013.07.050

MUC5AC constitutes the primary gel-forming component in gastric mucus, but is also a key constituent of cervical and airway mucus (2) and hence contributes to the mucus properties in these important anatomical locations. Hydrogels built from purified mucins have an important advantage over native mucus: they can be generated under defined conditions and with consistent properties, allowing repetitions of experiments under reproducible conditions. This is difficult to achieve with native mucus from individuals, which varies widely due to physiological differences between individual patients (onset of illness, age, nutrition, etc.). Moreover, MUC5AC-based hydrogels have proven valuable for the investigation of mucin gelation properties (24), microbial behavior in the mucus layer (25,26), and recreate critical permeability properties of native mucus toward nanoparticles (19,20) and protons (27).

We have engineered a microfluidic system, which allows for the detailed quantification of the partitioning and transport gradients of peptides (and nanoparticles) into a mucin-based barrier. Using these tools, we show that a combination of positive and negative surface charges leads to nonadditive effects on transport, and that nanoscale differences in the spatial charge configuration of the peptide surface can significantly affect the rate of transport. We also show that such selective transport is sensitive to ionic strength in the mucin barrier. These results significantly improve our understanding of the basic principles that govern selective transport through the mucin barrier, and have implications for the design of drug delivery vehicles for mucosal targeting.

MATERIALS AND METHODS

Mucin purification and sample preparation

Mucins were purified from scrapings of fresh pig stomachs according to the method developed by Gong et al. (28), with the difference that the cesium chloride density gradient centrifugation was omitted. Lyophilized mucins were reconstituted at 0.5% (w/v) in reconstitution buffer containing NaCl and Hepes (4-(2-hydroxyethyl)-1-piperazineethanesulfonic acid). Three NaCl/Hepes concentrations were used, including 5 mM NaCl/5 mM Hepes, 20 mM NaCl/20 mM Hepes, and 200 mM NaCl/20 mM Hepes. The reconstitution buffers used in all experiments were titrated to pH 7 using 6 M NaOH before dissolving of the mucins, and 0.0007% (w/v) of 500 nm fluorescent polystyrene microspheres (Polysciences, Warrington, PA) were added to the reconstituted mucin solution as a fluorescent tracer to track the flow of the mucins during microfluidic device filling. Hepes buffer at 20 mM has been previously used to reconstitute lyophilized mucins without affecting mucin viscoelasticity as measured using rheometry, suggesting that Hepes does not interfere with the molecular organization of mucins (19). The polystyrene particles added at a similar concentration to native mucus do not interfere with mucus permeability (14).

Fluorescent mucins were obtained by labeling the purified mucins with the Alexa488 fluorophore using the carboxylic acid succinimidyl ester amine-reactive derivatives (Life Technologies Corporation, Grand Island, NY). Mucins (4 mg/mL) were mixed with the dye in a carbonate-bicarbonate buffer (0.2 M, pH 8.5) at a protein/dye mass ratio of 1:40 for 1 h at room temperature. The excess dye was eliminated through multiple concentration-dilution cycles by centrifuge filtering (Pall Corporation, Port Washington, NY, 10 kDa MWCO).

Preparation of peptides

Peptides were synthesized by the Koch Institute Biopolymers and Proteomics Facility at MIT (Cambridge, MA). During synthesis, each peptide is labeled with one fluorescein molecule at the N-terminus. The synthesized peptides were desalted to remove trifluoroacetic acid remaining as a byproduct of the synthesis process using a PD MiniTrap G-10 (GE Healthcare, Piscataway, NJ) size exclusion column with 20 mM NaCl/20 mM Hepes at pH 7 as the equilibration and elution buffers. The eluted fractions at pH 7 are retained for experiments. The concentration of the purified peptide was determined by the absorption of the fluorescein-labeled peptides at the fluorescein excitation wavelength of 490 nm compared to a concentration standard with free fluorescein dye. Peptides were used at a final concentration of 4 μM in the permeability experiments. Identical concentrations of NaCl and Hepes were used for creating the mucin barrier and the peptide flow on-chip to avoid ionic concentration gradients, which could affect the barrier permeability properties.

Microfluidic device fabrication

Soft polymer microfluidic device fabrication techniques were used to fabricate the microfluidic devices (29). Two silicon wafer masters were created: one for the peptide flow and mucin channels, and another for the microfluidic valve. For the flow and mucin channels wafer, the microchannel features were defined in AZ4620 positive photoresist (Clariant Corporation, Somerville, NJ) coated onto a silicon wafer to a height of 30 μm, followed by baking on a hot plate for 1 h at 150°C for photoresist reflow to create the rounded channel profile needed for microfluidic valve activation (30). For the valves wafer, valve features were defined in SU8 negative photoresist (Microchem Corporation, Newton, MA) coated onto a silicon wafer to a height of 20 μm. Both finished wafers were treated with perfluorinated trichlorosilane (T2492-kg, United Chemical Technologies, Bristol, PA) in a desiccator jar for at least 4 h to prevent irreversible RTV bonding to the wafer.

RTV prepolymer and curing agent (RTV615, Momentive Performance Materials, Albany, NY) were mixed in a 1:5 (w/w) ratio, degassed for 1 h inside a desiccator jar, and poured onto the flow channels wafer to a height of ~1 cm. RTV prepolymer and curing agent were also mixed in a 1:20 (w/w) ratio, degassed for 1 h, and spun onto the valves wafer at 1200 rpm for 60 s, resulting in an RTV thin layer of ~60 μm. The two wafers were baked separately on hotplates at 95°C for 45 min, after which the partially cured RTV structures were peeled from the flow channels wafer and aligned to the valve features on the valves wafer with the aid of a dissection microscope. The valves wafer with the bonded flow channel RTV structures was placed on a hotplate at 95°C for at least 24 h to cure the monolithic RTV flow channels and valves structure. These structures were then peeled from the wafer and cut into individual devices. Finally, access holes for fluid connections to the sample channels are punched, and the RTV structure was bonded to a glass slide after treatment with oxygen plasma to complete the device.

The bonded device is mounted onto an inverted epifluorescence microscope (IX-71, Olympus American, Central Valley, PA). Pipette tips with 200 μL volume (USA Scientific, Ocala, FL) were modified by cutting off a 2 mm section from the tip and then inserting it into the punched RTV access holes to function as fluid reservoirs. A 3 mL plastic syringe is connected through PTFE tubing (IDEX Health & Science LLC, Oak Harbor, WA) to the valve channel reservoir, allowing pneumatic control of the microfluidic valve. The reconstituted mucin sample is loaded into a 50 μL volume glass syringe (model 1705, Hamilton Company, Reno, NV) and connected to the device through a 15 cm length of fused silica tubing (Fused Silica Tubing TSP 0.36 mm outer diameter/100 μm inner diameter, Polymicro Technologies, Phoenix, AZ). Peptide flow rates were set using gravity driven flow by filling an inlet and outlet peptide reservoir to uneven heights. The same flow rate was used for all experiments.

Mucin barrier formation on-chip and experiment procedure

Fig. 1 *a* shows the top-down geometry of the microfluidic device used to form the mucin barrier. The device design consists of a wide main channel (200 μm wide by 30 μm high) with a side channel (75 μm wide by 30 μm high). The main channel contains a push down style (30) microfluidic valve ~450 μm from the intersection of the main and side channels. This valve may be reversibly opened or closed based on applied air pressure inside the valve channel. To operate the device, the mucin sample is pumped into the device and fills both the main channel and the side channel while the valve is open. In step 2, the microfluidic valve is closed, and a buffer solution is flowed by gravity into the flow channel and out the top of the main channel, flushing away mucins in its flow path and creating a mucin-water interface. We define the location of this interface to $x = 0$. In step 3, the buffer flow in the side channel is replaced by a flow of the fluorescent peptide molecules. These peptides then diffuse into the mucin barrier across the water-mucin interface.

Data acquisition and analysis

Fluorescent images of peptide transport into the mucin barrier were obtained at 10 s intervals. To prevent photobleaching, the excitation light-emitting diode of the microscopy system was programmatically set to only turn on during active exposure. From each fluorescence image, the fluorescence profile of the peptide is extracted across the midline of the mucin channel (see the *dotted line* in Fig. 2 *b*), subtracting the background fluorescence, and converted to a concentration profile assuming linearity between concentration and fluorescence as demonstrated in previous microfluidic experiments (31).

Each peptide accumulation into the mucin barrier is calculated by integrating the cross-sectional peptide concentration profile as a function of x for the range of x values covering the width of the mucin barrier and dividing by the width of the mucin barrier. This calculates the average peptide concentration accumulated inside the mucin barrier over the duration of experiment.

All error bars and $\pm$ error values given in the text and figures represent one standard deviation. A minimum of three experiments were conducted for each data point.

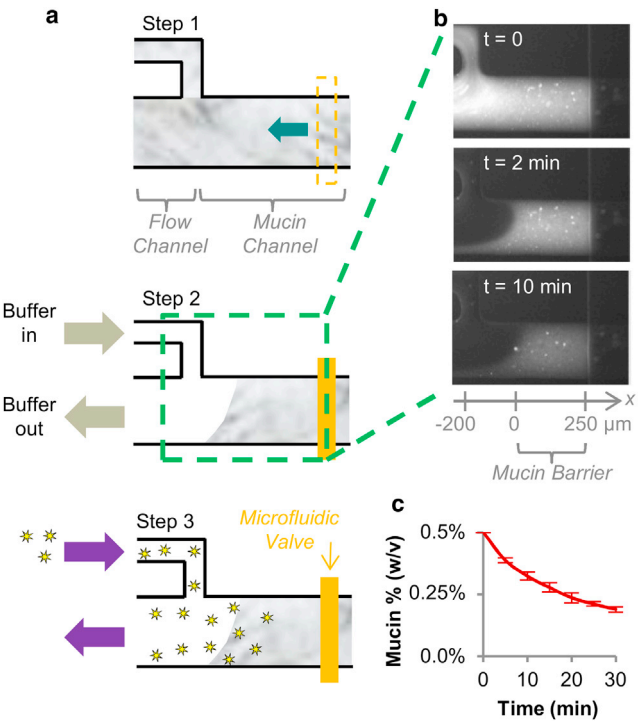

FIGURE 1 Microfluidic device enables mucin barrier formation on-chip. (*a*) A mucin sample initially filling both the flow and mucin channels (step 1, *top-down view*) is shaped into a layer of fixed width between a buffer flow and a microfluidic valve inside the mucin channel (step 2). Fluorescent peptides flushed into the device arrive at the mucin barrier surface and transport into the mucin barrier over time. (step 3) (*b*) Formation and stability of the mucin barrier on-chip is assessed using fluorescently labeled mucins, showing that the mucin barrier surface interface is stable over time. (*c*) Mucins are gradually lost from the mucin barrier over time, likely due to surface fluid shearing. We limit the duration of permeability measurements to 10 min to ensure that a majority of the initial mucin quantity remains inside the mucin barrier during the experiment. $n = 3$ devices.

RESULTS AND DISCUSSION

Microfluidic device enables the formation of a mucin barrier on-chip

The passage of a particle across the mucus barrier consists of a series of events, including partitioning (or entry) into the mucus barrier, translocation through the barrier, and exit from the barrier. Several studies have used multiple particle tracking techniques (10–20) or fluorescence recovery after photobleaching (32,33) to measure the diffusivity of particulates inside the mucus gel. These techniques reveal important information about the mobility of particles inside the mucus barrier, but they lack information about a particle's ability to enter the mucus barrier. This information is crucial to predict overall transport through any barrier. To address this technical limitation we have created a microfluidic system with which we can generate a mucin barrier on-chip, and quantify particles entry into, and transport across, the mucin barrier (Fig. 1 *A*).

The mucin sample is filled into the microfluidic device (Fig. 1 *a*, step 1, *top-down view*) and shaped into a barrier of ~250 μm width, using buffer flow (*left*) and a microfluidic valve (*right*) (step 2). To determine the stability of the on-chip barrier, we spiked the mucin sample with fluorescently labeled mucins and monitored both the presence of the mucin barrier interface and the fluorescence intensity of the barrier over time (Fig. 1 *b*). This experiment revealed that the interface of the mucin barrier remains stable over the entire time of observation. However, over time, the concentration of mucins inside the barrier appears to decrease (Fig. 1 *c*), likely due to fluid shearing at the mucin barrier interface. This shedding process also occurs in the natural mucus layer in vivo due to enzyme action and fluid shearing (34), and could provide valuable information, but it also complicates the quantification of transport. Hence, to avoid this complication we limit the duration of the transport experiments to 10 min, where we observe a minimal shedding of the barrier.

Mucins form a charge selective permeability barrier to peptides

To study the effect of detailed spatial arrangements and combination of charge on mucosal passage, we need to

test substrates that can be equipped with defined heterogeneous spatial surface configurations. This is not easy to achieve with nanoparticles, hence, we explored if short peptides, which are easy to manipulate and allow for a systematic variation of amino acid arrangements, may serve as alternative reporters for probing mucin-barrier selectivity. We prepared two peptides with uniform charge: the cationic peptide consisted of 10 positively charged lysine residues, each separated by one alanine residue; and the anionic peptide consisted of 10 negatively charged glutamic acid residues, each also separated by one alanine residue. Each peptide was labeled with one fluorescein molecule for visualization (Fig. 2 *a*).

We quantified the transport of the cationic and anionic peptides into a barrier consisting of 0.5% mucins (w/v; reconstituted in 20 mM NaCl/20 mM Hepes) (Fig. 2, *b* and *c*). The peptides were introduced into the microfluidic channel at a concentration of 4 μM. At this concentration, the peptides represented a minority of the charge in the system and hence, would not significantly change the ionic environment of the mucin barrier. Fluorescence micrographs and the peptide transport profiles are shown in Fig. 2, *b* and *c*. Fig. 2 *c* indicates that the anionic peptide forms a decreasing concentration gradient through the mucin barrier that looks similar to the profile established in the absence of mucins. This result suggests a near lack of interactions between this peptide and the mucins. This conclusion was confirmed by quantifying the average concentration of the peptide that accumulated inside the mucin barrier over 10 min (see Fig. 3 *b*). This quantification shows

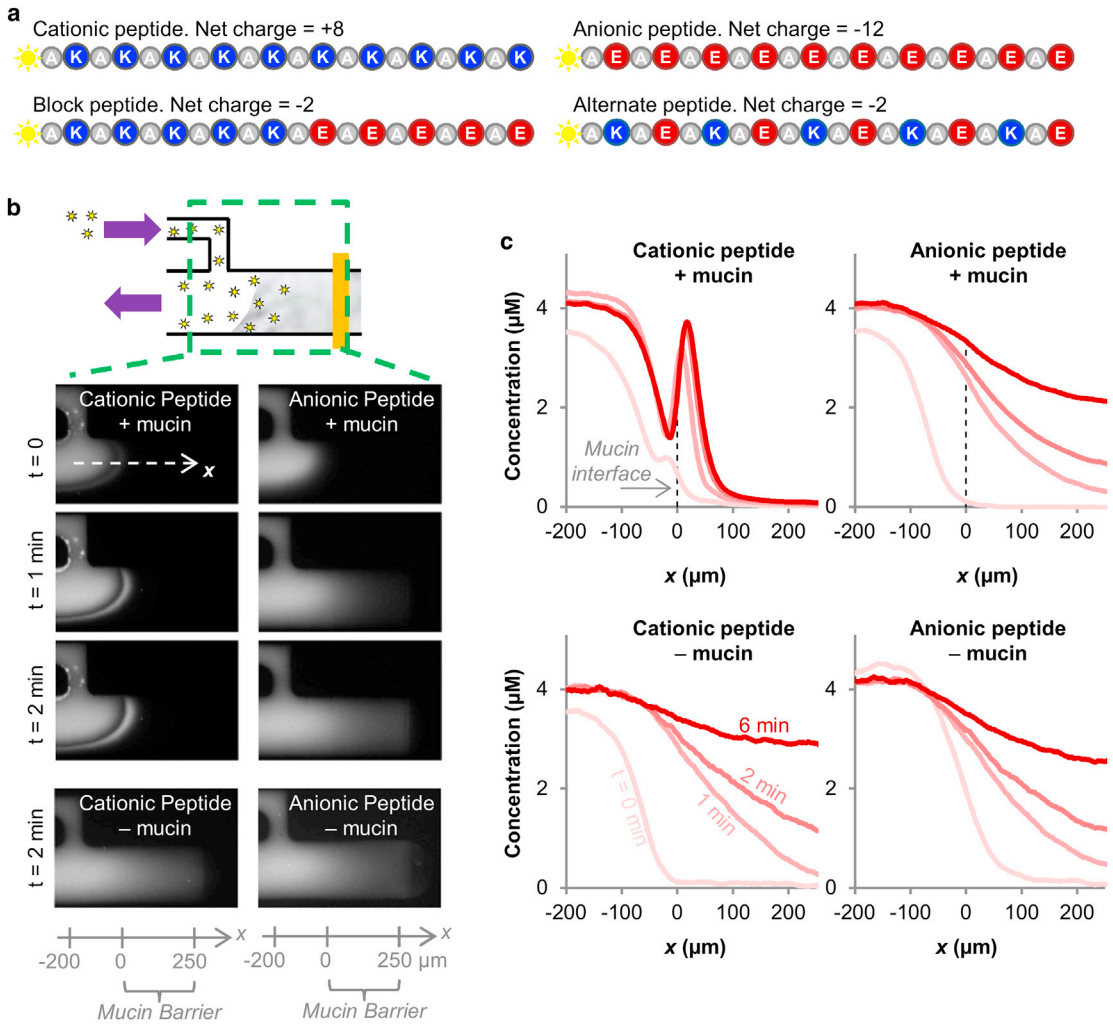

FIGURE 2 Mucins form a charge selective permeability barrier to peptides. (*a*) A suite of peptides of equal molecular weight but with different net charge and spatial charge distributions are used as probes to test mucin barrier permeability. Note the block and alternate peptides are molecular isomers. (*b*) Time series of fluorescence peptides entering a 0.5% (w/v) mucin barrier at 20 mM NaCl ionic strength show different transport behaviors of the cationic and anionic peptides. (*c*) Fluorescence images are analyzed across the midline of the microfluidic mucin channel (marked by *dotted arrow labeled x* in Fig. 2 *b*) to obtain peptide concentration profiles in the absence and presence of 0.5% (w/v) mucins. The peptide profiles of the two peptides differ in the presence of mucins but are shaped identically when mucins are absent, demonstrating that mucins are responsible for the selective transport of the peptides.

that transport of the anionic peptide was reduced by 12% in the presence of the mucins (from 3.3 ± 0.2 μM to 2.9 ± 0.1 μM).

The situation was different for the cationic peptide, whose concentration rose to a peak value at the entry of the mucin barrier, before sharply dropping off. (Fig. 2 *c*) This peak is indicative of attractive interactions between the cationic peptide and negatively charged mucins, or possible mucin barrier surface partitioning effects such as Donnan partitioning (35,36) that would enhance local peptide concentration. The quantification of accumulation reveals that the concentration of cationic peptide inside the mucin barrier was reduced by 61% compared to the same region in the mucin-free control (Fig. 3 *a*, from 3.3 ± 0.1 μM to 1.3 ± 0.1 μM), showing that the mucins strongly hinder free diffusion of the cationic peptide. Taken together, these results confirm previous studies that show particulate net charge strongly influences transport through the mucin barrier (20). Hence, we conclude that short peptides, despite their small size, reflect critical transport properties observed with uniformly coated nanoparticles and hence, are useful reporters for further probing mucin permeability mechanisms.

A combination of negative and positive surface charge results in accelerated peptide transport

Having confirmed the selective transport of peptides based on charge, we next tested the effect of combining positive and negative charges within the same peptide. For this experiment we generated block peptides, which consist of five positively charged amino acids followed by five negatively charged amino acids, with alanine residue spacers interspersed between the charged amino acids (Fig. 2 *a*). Transport of the block peptide was measured using the microfluidic system under the same conditions as in Fig. 2 and Fig. 3, *a* and *b*.

Because half of the block peptide is positively charged and the other half is negatively charged, it is tempting to speculate that its transport rate would be the additive average of the cationic and anionic peptide transport rates. However, Fig. 3 shows that this is not the case. Instead, the combination of positive and negative surface charge leads to enhanced transport compared to either surface charge in isolation: The concentration of the block peptide that entered the mucin barrier amounted to 300% of the concentration reached by the purely cationic peptide

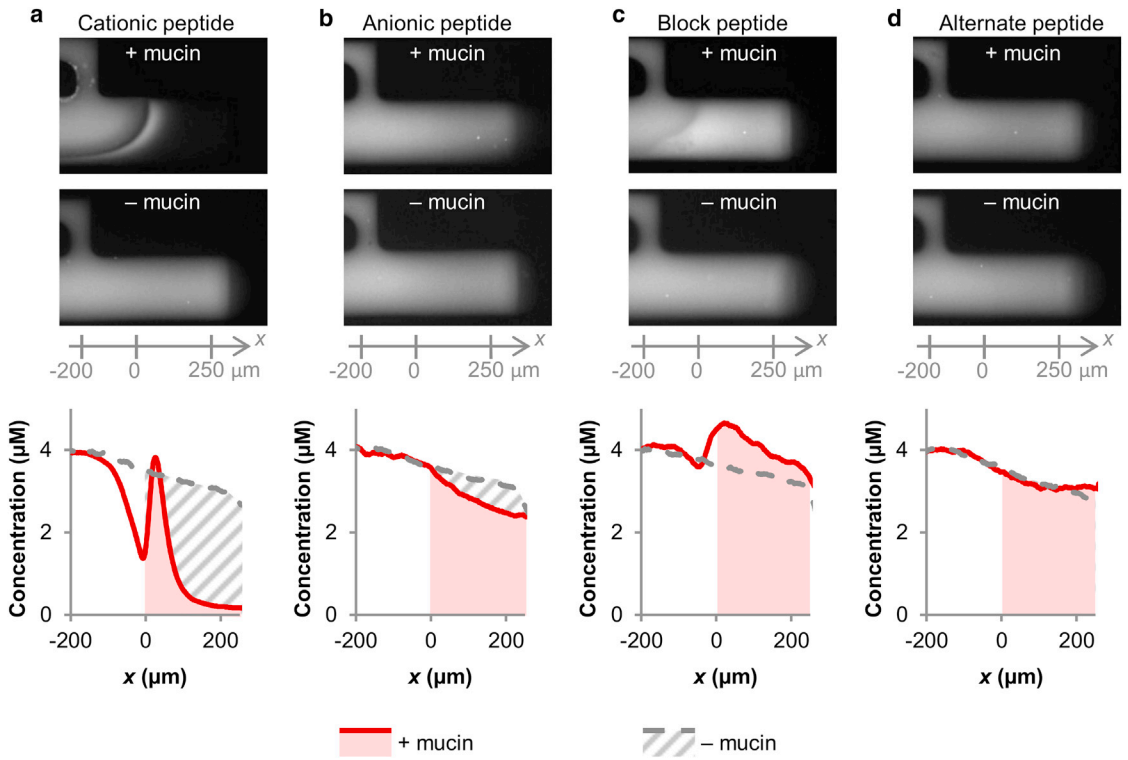

FIGURE 3 Specific spatial distributions of negative and positive surface charge can accelerate peptide transport into a mucin barrier at an ionic strength of 20 mM. Quantification of peptide accumulation inside the mucin barrier and in mucin-free buffer after 10 min. (*a* and *b*) Cationic peptide transport was strongly reduced, while anionic peptide transport was only marginally reduced by the presence of mucins. (*c*) Peptides composed of cationic and anionic blocks (5 amino acids each) reach higher concentrations in the mucin barrier compared to free diffusion in the buffer control, suggesting that the mucins promote transport of these peptides. (*d*) Transport of the alternate peptide, a molecular isomer of the block peptide, shows no mucin dependent change in transport rate. This indicates that the detailed charge distribution is critical for the transport properties of the peptide. (Movie S1 in the Supporting Material)

(4.0 ± 0.1 μM and 1.3 ± 0.1 μM, respectively; Fig. 3, *a* and *c*), and to 140% of the concentration reached with the purely anionic peptide during the same time (2.9 ± 0.1 μM; Fig. 3 *b*). Fig. 3 *c* also shows that the block peptide accumulated to a higher concentration inside the mucin barrier than inside the mucin-free control chamber (4.0 ± 0.1 μM with mucins vs. 3.4 ± 0.1 μM without mucins,). Together, these results suggest that the transport of the block peptide is enhanced by the presence of the mucins, whereas the transport of both the cationic and anionic peptides is slowed by the mucins. This observation implies that the mucins may facilitate the transport of heterogeneously charged substrates, although hindering the transport of uniformly charged substrates.

The finding that combined positive and negative surface charges can lead to facilitated transport in mucin environments has important in vivo implications. Viruses contain combinations of positive and negative surface charges that may modulate interactions between the particle and the mucosal barrier (22,37). Soluble proteins such as those secreted by bacteria also contain heterogeneous surface charges, which may have evolved to interact with the mucus barrier (21). Drug and gene carriers may also be multifunctionalized with positive and negative charges to control transport and targeting in the mucus barrier.

We speculate that several mechanisms contribute to the nonadditive selective transport effects of the block peptide. For example, particle charge can dramatically alter the partitioning of a substrate into a solution/gel interface via the Donnan/Boltzmann partitioning factor (35,36). This partitioning can, in principle, accelerate transport for net-positively charged peptides and slow transport of negative particles into a gel composed of negatively charged polymers such as mucins. At the same time, if positive charge on the particle leads to binding to mucins, the resulting diffusion-reaction kinetics can dramatically slow transport of particles through the mucin layer, despite Donnan partitioning. Both mechanisms may interact in complex ways to produce the selective permeability effect we observed among the cationic, anionic, and block peptides. In the future, experimental methods and theoretical models (38) that independently quantify the effects of partitioning, binding, and the resulting transport kinetics may be adapted to mucin materials and to the microfluidics system to quantify the relative effects of each mechanism component, and to determine the relative quantities of bound and free peptides in the mucin barrier.

Spatial charge distribution influences peptide transport

Having established that the combination of positive and negative charges can result in nonadditive transport effects, we now asked whether the detailed spatial arrangement of surface properties would influence permeability into a mucin barrier. This question is important because the spatial arrangement of positive and negative charges on the surfaces of viruses and native proteins can also naturally vary (21,22), and tuning of spatial charge distributions on drug and gene carriers may provide the practical benefit of transport and targeting control in the mucus barrier. To determine if spatial charge configuration influences permeability properties of the mucin barrier, we measured the transport of a peptide, which contains the identical amino acids as the block peptide but arranged in an alternating sequence, as opposed to separate blocks. (Fig. 2 *a*) Fig. 3, *c* and *d*, shows that transport of the alternate peptide differed from that of the block peptide in two measurable ways: First, its transport profile into the mucin barrier was monotonically descending, without a discernable peak as was observed for the block peptide. Second, its accumulation rate was unaffected by the presence of mucins (3.2 ± 0.1 μM inside a mucin barrier vs. 3.3 ± 0.2 μM in the absence of mucins). These differences between the transport profiles and transport rates of the block and alternate peptides show that the mucin barrier can distinguish the spatial configuration of charged residues on a nanometer length scale, and that the transport behavior through the mucin barrier cannot be predicted by net charge of a substrate alone.

The ionic environment of the mucin barrier regulates selective permeability

The ionic strength of the mucus barrier varies in different anatomical locations (39), is altered by the menstrual cycle (40), and becomes dysregulated in diseases such as cystic fibrosis (41). The pH of mucus also varies from very acidic in the stomach (42) to neutral in the respiratory airways (43) and cervix (44). Such differences in the ionic strength and environment of the mucus layer have previously been proposed as a method used by the body to rapidly tune the selective permeability function of the mucus barriers (19). This background and our findings that charge composition and configuration strongly influence transport through mucin gels led us to test if altered ionic strength may affect selective peptide transport. We varied the NaCl concentration in the mucin samples and measured the resulting transport of the suite of four peptides used previously. At high ionic strength (200 mM NaCl), the cationic peptide accumulated to a ninefold higher concentration compared to at low ionic strength (5 mM NaCl; from 0.4 ± 0.1 μM at 5 mM NaCl to 4.0 ± 0.2 μM at 200 mM NaCl; Fig. 4 *a*). For comparison, the anionic peptide only enriched 0.2 fold at 200 mM NaCl compared to the low ionic strength conditions (Fig. 4 *a*). Hence, ionic strength strongly influences transport of the cationic peptide, whereas the anionic peptide remains largely unaffected.

This series of experiments also revealed that the transport rate for the block peptide was highest at an intermediate ionic strength of 20 mM NaCl (4.0 ± 0.1 μM), compared

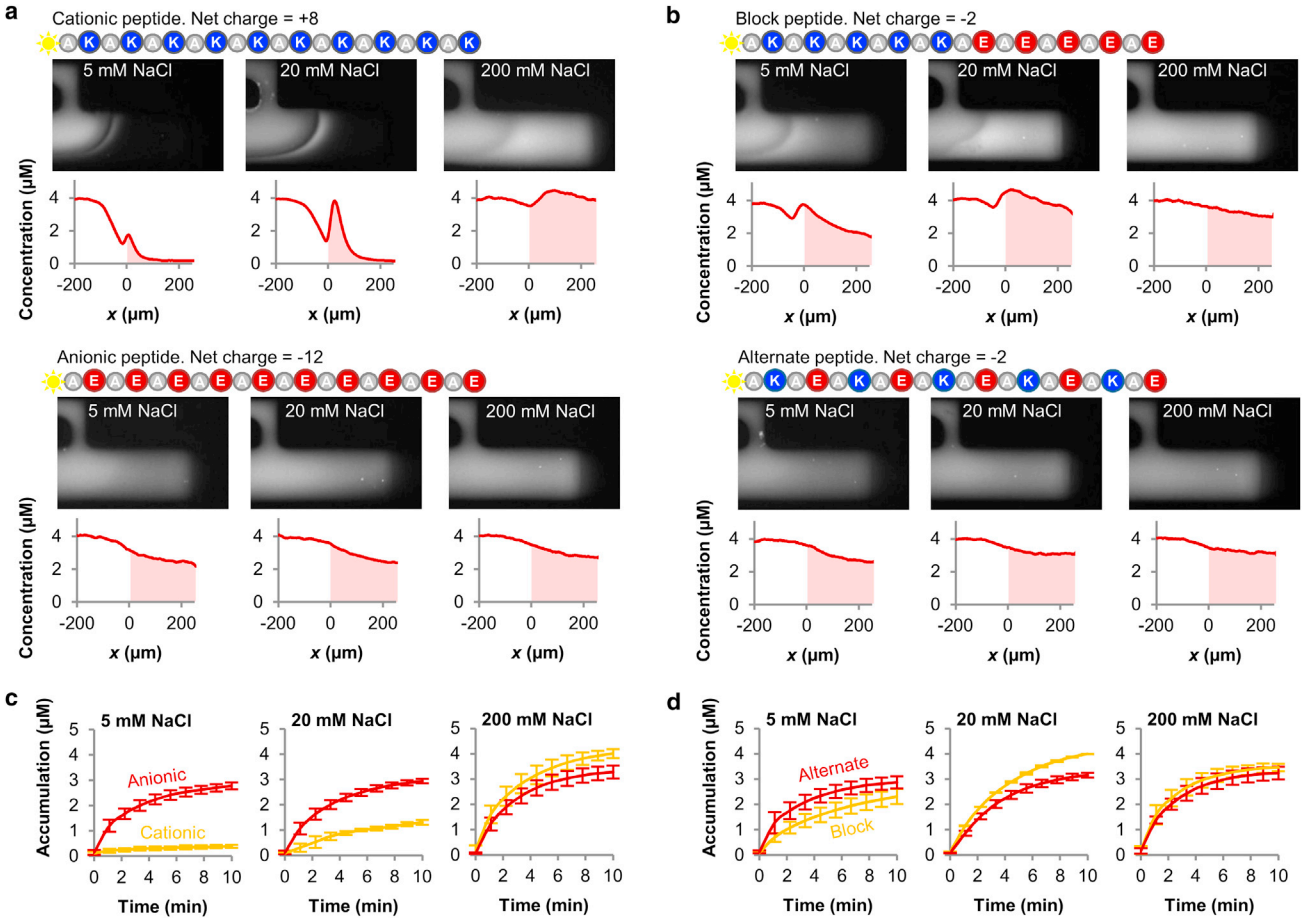

FIGURE 4 The ionic strength of the mucin barrier can regulate its selective properties. (*a*) Increasing ionic strength within the mucin barrier significantly increases penetration and transport of the cationic (ninefold increase in accumulation from 5 to 200 mM ionic strength), but only marginally increases transport of the anionic peptide. (*b*) Unlike the uniformly charged cationic and anionic peptides whose transport rates increased monotonically with ionic strength, the transport rate of the block peptide was highest at the intermediate ionic strength of 20 mM NaCl. The transport rate of the alternate peptide was not significantly affected by ionic strength, demonstrating that the influence of ionic strength on peptide transport depends on spatial distribution of change. (Movie S2 and Movie S3) (*c* and *d*) The transport rates of the individual peptide species relative to one another depend on the surrounding ionic strength. Hence, charge polarity and distribution may be tuned to maximize transport into mucus barriers at different anatomical locations with varying ionic environments. $n \geq 3$ for each peptide and ionic strength combination.

to 2.3 ± 0.3 μM at 5 mM NaCl, and 3.5 ± 0.2 μM at 200 mM NaCl (Fig. 4 *b*). Hence, although transport of cationic and anionic peptides into the mucin barrier monotonically increased with ionic strength, the block peptide showed maximal transport at an intermediate value. The alternate peptide, in contrast, was not measurably affected by ionic strength and accumulated to 3.1 ± 0.2 μM at all three salt concentrations (Fig. 4 *b*). Together, these results suggest that the influence of ionic strength on transport not only depends on the type of charge present in the peptide, but also on its detailed arrangement. This implies that the charge polarity and distribution can be optimized to maximize transport into a mucin barrier at different mucus ionic environments: At low ionic strength (5 mM NaCl), the anionic and alternate peptides transported fastest, at intermediate ionic strengths (20 mM NaCl) the block peptide transported most effectively, and at high ionic strength (200 mM NaCl) the cationic peptide accumulated most effectively (Fig. 4, *c* and *d*).

Taken together, our findings have important physiological implications. For example, they suggest that pathogens such as certain viruses may adopt their surface properties to tune interactions with mucins and thereby perfect transport through mucus barriers at certain anatomical locations. In addition, our results imply that drug and gene carriers may be equipped with specific surface charge configurations to optimize their interactions with the mucins in mucus barriers of varying ionic strength or pH arising from diseases such as cystic fibrosis and gastric ulcers. In the future, our experimental system can be used to probe other parameters relevant for permeability, such as hydrophobicity. Moreover, different types of mucins such as from lung or cervical mucus, as well as additional mucus components including lipids, DNA, antibodies, and antimicrobial peptides can be

studied to understand the mechanisms of the mucus barrier permeability in more detail. The microfluidic system presented here also enables the study of small volumes of primary native mucus, which will be valuable to correlate permeability changes to mucosal diseases.

SUPPORTING MATERIAL

Three movies and their legends are available at http://www.biophysj.org/biophysj/supplemental/S0006-3495(13)00875-8.

We thank Prof. Alan Grodzinsky for invaluable discussions and advice.

This work was in part supported by a fellowship from the Martinos Scholars fund at the Harvard-MIT Division of Health Sciences and Technology, the National Research Foundation (Singapore) through the Singapore-MIT Alliance for Research and Technology (SMART) Centre (BioSyM and ID IRG), MIT faculty startup funds for K.R., a Marie Curie International Outgoing Fellowship "BIOMUC" to T.C., and a postdoctoral fellowship from Johnson and Johnson Services Inc. to L.L.

REFERENCES

1. Lieleg, O., and K. Ribbeck. 2011. Biological hydrogels as selective diffusion barriers. *Trends Cell Biol.* 21:543–551.
2. Linden, S. K., P. Sutton, …, M. A. McGuckin. 2008. Mucins in the mucosal barrier to infection. *Mucosal Immunol.* 1:183–197.
3. McGuckin, M. A., S. K. Lindén, …, T. H. Florin. 2011. Mucin dynamics and enteric pathogens. *Nat. Rev. Microbiol.* 9:265–278.
4. Thornton, D. J., and J. K. Sheehan. 2004. From mucins to mucus: toward a more coherent understanding of this essential barrier. *Proc. Am. Thorac. Soc.* 1:54–61.
5. Tabak, L. A., M. J. Levine, …, S. A. Ellison. 1982. Role of salivary mucins in the protection of the oral cavity. *J. Oral Pathol.* 11:1–17.
6. Boucher, R. C. 2007. Airway surface dehydration in cystic fibrosis: pathogenesis and therapy. *Annu. Rev. Med.* 58:157–170.
7. Hollingsworth, M. A., and B. J. Swanson. 2004. Mucins in cancer: protection and control of the cell surface. *Nat. Rev. Cancer.* 4:45–60.
8. Oppenheimer, E. A., A. L. Case, …, R. M. Rothberg. 1970. Cervical mucus in cystic fibrosis: a possible cause of infertility. *Am. J. Obstetrics Gynecol.* 108:673–674.
9. Poon, W. W., and J. A. McCoshen. 1985. Variances in mucus architecture as a cause of cervical factor infertility. *Fertil. Steril.* 44:361–365.
10. Dawson, M., D. Wirtz, and J. Hanes. 2003. Enhanced viscoelasticity of human cystic fibrotic sputum correlates with increasing microheterogeneity in particle transport. *J. Biol. Chem.* 278:50393–50401.
11. Dawson, M., E. Krauland, …, J. Hanes. 2004. Transport of polymeric nanoparticle gene carriers in gastric mucus. *Biotechnol. Prog.* 20:851–857.
12. Tang, B. C., M. Dawson, …, J. Hanes. 2009. Biodegradable polymer nanoparticles that rapidly penetrate the human mucus barrier. *Proc. Natl. Acad. Sci. USA.* 106:19268–19273.
13. Wang, Y. Y., S. K. Lai, …, J. Hanes. 2008. Addressing the PEG mucoadhesivity paradox to engineer nanoparticles that "slip" through the human mucus barrier. *Angew. Chem. Int. Ed. Engl.* 47:9726–9729.
14. Wang, Y. Y., S. K. Lai, …, J. Hanes. 2011. Mucoadhesive nanoparticles may disrupt the protective human mucus barrier by altering its microstructure. *PLoS ONE.* 6:e21547.
15. Lai, S. K., D. E. O'Hanlon, …, J. Hanes. 2007. Rapid transport of large polymeric nanoparticles in fresh undiluted human mucus. *Proc. Natl. Acad. Sci. USA.* 104:1482–1487.
16. Lai, S. K., Y. Y. Wang, and J. Hanes. 2009. Mucus-penetrating nanoparticles for drug and gene delivery to mucosal tissues. *Adv. Drug Deliv. Rev.* 61:158–171.
17. Lai, S. K., Y. Y. Wang, …, J. Hanes. 2010. Nanoparticles reveal that human cervicovaginal mucus is riddled with pores larger than viruses. *Proc. Natl. Acad. Sci. USA.* 107:598–603.
18. Cu, Y., and W. M. Saltzman. 2009. Controlled surface modification with poly(ethylene)glycol enhances diffusion of PLGA nanoparticles in human cervical mucus. *Mol. Pharm.* 6:173–181.
19. Lieleg, O., I. Vladescu, and K. Ribbeck. 2010. Characterization of particle translocation through mucin hydrogels. *Biophys. J.* 98:1782–1789.
20. Crater, J. S., and R. L. Carrier. 2010. Barrier properties of gastrointestinal mucus to nanoparticle transport. *Macromol. Biosci.* 10:1473–1483.
21. Wada, A., and H. Nakamura. 1981. Nature of the charge distribution in proteins. *Nature.* 293:757–758.
22. Cone, R. A. 2009. Barrier properties of mucus. *Adv. Drug Deliv. Rev.* 61:75–85.
23. Reference deleted in proof.
24. Celli, J. P., B. S. Turner, …, S. Erramilli. 2007. Rheology of gastric mucin exhibits a pH-dependent sol-gel transition. *Biomacromolecules.* 8:1580–1586.
25. Celli, J. P., B. S. Turner, …, R. Bansil. 2009. *Helicobacter pylori* moves through mucus by reducing mucin viscoelasticity. *Proc. Natl. Acad. Sci. USA.* 106:14321–14326.
26. Caldara, M., R. S. Friedlander, …, K. Ribbeck. 2012. Mucin biopolymers prevent bacterial aggregation by retaining cells in the free-swimming state. *Curr. Biol.* 22:2325–2330.
27. Li, L., O. Lieleg, …, J. Han. 2012. A microfluidic in vitro system for the quantitative study of the stomach mucus barrier function. *Lab Chip.* 12:4071–4079.
28. Gong, D. H., B. Turner, …, J. T. Lamont. 1990. Lipid binding to gastric mucin: protective effect against oxygen radicals. *Am. J. Physiol.* 259:G681–G686.
29. Duffy, D. C., J. C. McDonald, …, G. M. Whitesides. 1998. Rapid Prototyping of Microfluidic Systems in Poly(dimethylsiloxane). *Anal. Chem.* 70:4974–4984.
30. Unger, M. A., H.-P. Chou, …, S. R. Quake. 2000. Monolithic microfabricated valves and pumps by multilayer soft lithography. *Science.* 288:113–116.
31. Cheow, L. F., and J. Han. 2011. Continuous signal enhancement for sensitive aptamer affinity probe electrophoresis assay using electrokinetic concentration. *Anal. Chem.* 83:7086–7093.
32. Olmsted, S. S., J. L. Padgett, …, R. A. Cone. 2001. Diffusion of macromolecules and virus-like particles in human cervical mucus. *Biophys. J.* 81:1930–1937.
33. Saltzman, W. M., M. L. Radomsky, …, R. A. Cone. 1994. Antibody diffusion in human cervical mucus. *Biophys. J.* 66:508–515.
34. Johansson, M. E. 2012. Fast renewal of the distal colonic mucus layers by the surface goblet cells as measured by in vivo labeling of mucin glycoproteins. *PLoS ONE.* 7:e41009.
35. Grodzinsky, A. J. 2011. Fields, Forces, and Flows in Biological Systems, 1st ed. Garland Science, New York.
36. Donnan, F. 1911. The theory of membrane equilibrium in the presence of a non-dialyzable electrolyte. *Z Elektrochem.* 17:572–581.
37. Cone, R. A. 2005. Mucus. *In* Mucosal Immunology, 3rd ed. J. Mestecky, M. E. Lamm, W. Strober, J. Bienenstock, J. R. McGhee, and L. Mayer, editors. Academic Press, Burlington, MA, pp. 49–72.
38. Byun, S., M. D. Tortorella, …, A. J. Grodzinsky. 2010. Transport and equilibrium uptake of a peptide inhibitor of PACE4 into articular cartilage is dominated by electrostatic interactions. *Arch. Biochem. Biophys.* 499:32–39.

39. Knowles, M. R., J. M. Robinson, …, R. C. Boucher. 1997. Ion composition of airway surface liquid of patients with cystic fibrosis as compared with normal and disease-control subjects. *J. Clin. Invest.* 100:2588–2595.

40. Gould, K. G., and A. H. Ansari. 1981. Electrolyte interactions in cervical mucus and their relationship to circulating hormone levels. *Contraception.* 23:507–516.

41. Kozlova, I., V. Vanthanouvong, …, G. M. Roomans. 2006. Composition of airway surface liquid determined by X-ray microanalysis. *Ups. J. Med. Sci.* 111:137–153.

42. Ovesen, L., F. Bendtsen, …, S. J. Rune. 1986. Intraluminal pH in the stomach, duodenum, and proximal jejunum in normal subjects and patients with exocrine pancreatic insufficiency. *Gastroenterology.* 90:958–962.

43. Karnad, D. R., D. G. Mhaisekar, and K. V. Moralwar. 1990. Respiratory mucus pH in tracheostomized intensive care unit patients: effects of colonization and pneumonia. *Crit. Care Med.* 18:699–701.

44. Eggert-Kruse, W., A. Köhler, …, B. Runnebaum. 1993. The pH as an important determinant of sperm-mucus interaction. *Fertil. Steril.* 59:617–628.